Constitutive Silencing of LRRK2 Kinase Activity Leads to Early Glucocerebrosidase Deregulation and Late Impairment of Autophagy *in vivo*

Federica Albanese
  University of Ferrara: Universita degli Studi di Ferrara

Daniela Mercatelli
  University of Ferrara: Universita degli Studi di Ferrara

Luca Finetti
  University of Ferrara: Universita degli Studi di Ferrara

Giulia Lamonaca
  EURAC Center for Biomedicine: EURAC Centro di Biomedicina

Sara Pizzi
  EURAC Center for Biomedicine: EURAC Centro di Biomedicina

Derya Shimshek
  Novartis Pharma AG

Giovanni Bernacchia
  University of Ferrara: Universita degli Studi di Ferrara

Michele Morari (✉ mri@unife.it)
  University of Ferrara   https://orcid.org/0000-0002-4601-4454

Research article

Abstract

Background: Mutations in leucine-rich repeat kinase 2 (LRRK2) are associated with familiar and sporadic Parkinson's disease. LRRK2 modulates the autophagy-lysosome pathway (ALP), a clearance process subserving the quality control of cellular proteins and organelles. Since dysfunctional ALP might lead to α-synuclein accumulation and, hence, Parkinson's disease, LRRK2 kinase modulation of ALP, its age-dependence and relation with pSer129 a-synuclein inclusions in striatal and nigral neurons were investigated *in vivo*.

Methods: Striatal ALP markers were analyzed by Western blotting in 3, 12 and 20-month-old LRRK2 G2019S knock-in mice (bearing enhanced kinase activity), LRRK2 knock-out mice, LRRK2 D1994S knock-in (kinase-dead) mice and wild-type controls. The lysosomotropic agent chloroquine was used to investigate the autophagic flux *in vivo*. Quantitative Real-time PCR was used to quantify the transcript levels of key ALP genes. The activity of the lysosomal enzyme glucocerebrosidase was measured using enzymatic assay. Immunohistochemistry was used to co-localize LC3B puncta with pSer129 a-synuclein inclusion in striatal MAP-positive and nigral TH-positive neurons.

Results: No genotype differences in macroautophagy and chaperone-mediated autophagy markers were observed at 3 months. Conversely, increase of LC3-I, p62, LAMP2 and GAPDH levels, decrease of p-mTOR levels and downregulation of *mTOR* and *TFEB* expression was observed in 12-month-old kinase-dead mice. The LC3-II/LC3-I ratio was reduced following administration of chloroquine, suggesting a defective autophagic flux. G2019S knock-in mice showed LAMP2 accumulation and downregulation of ALP key genes *MAP1LC3B*, *LAMP2*, *mTOR*, *TFEB* and *GBA1*. Subacute administration of the LRRK2 kinase inhibitor MLi-2 in wild-type and G2019S knock-in mice did not replicate the pattern of kinase-dead mice. Lysosomal glucocerebrosidase activity was increased in 3 and 12-month-old knock-out and kinase-dead mice, and *GBA1* expression reduced in 12-month-old G2019S knock-in mice. Immunofluorescence revealed a dissociation between LC3B puncta accumulation and pSer129 a-synuclein inclusions in striatal neurons of kinase-dead and G2019S knock-in mice.

Conclusions: We conclude that constitutive LRRK2 kinase silencing results in early deregulation of GCase activity followed by late impairment of macroautophagy and chaperone-mediated autophagy. In G2019S knock-in mice, pSer129 a-synuclein inclusions observed under basal conditions appear unrelated to autophagy impairment.

Background

Accumulation of misfolded protein and damaged/dysfunctional organelles is a common hallmark of neurodegenerative disorders of aging, such as Parkinson's disease (PD). Several genetic factors, among which mutations in the leucine-rich repeat kinase 2 (*LRRK2*) gene, contribute to PD pathogenesis [1–3]. LRRK2 is a large multidomain protein, encompassing a catalytic core with GTPase and kinase domains, flanked by protein-protein interaction motifs [4, 5]. LRRK2-related PD is characterized by an age-

dependent and incomplete penetrance. The most common mutation, p.G2019S, confers enhanced kinase activity and causes autosomal dominant PD, whereas the *LRRK2* locus is a risk factor for idiopathic PD [6, 7]. The enhancement of LRRK2 kinase activity proved neurotoxic in several *in vitro* and *in vivo* studies [8–11]. On the contrary, LRRK2 mutant mice harboring kinase-dead mutations, among which D1994N, exhibited a reduced age-related neuronal toxicity [12]. LRRK2 plays a role in a variety of cellular functions and pathways, thus, not surprisingly, various mechanisms have been recognized or hypothesized to be involved in LRRK2-mediated neuropathology, among which the modulation of the autophagy-lysosomal pathway (ALP) [13–17]. Autophagy is a highly conserved process responsible for bulk degradation of cellular debris as well as dysfunctional/damaged organelles by delivery to lysosomes and is classically divided in three main types: macroautophagy, chaperone-mediated autophagy (CMA) and microautophagy. ALP integrates extracellular and intracellular stimuli to regulate energy balance and proteostasis [18, 19]. However, ALP efficiency declines during physiological aging [20], resulting in impaired α-synuclein (α-syn) clearance and, possibly, sensitization to PD onset or facilitation of its progression [21, 22]. Several studies have attempted to establish whether LRRK2 is a positive or negative modulator of ALP [14, 15, 23, 24]. Most studies were carried out *in vitro* and led to inconsistent data, possibly due to the different cell types and neurons used, type of LRRK2 mutant, and mutant overexpression levels. Also *in vivo* (*ex vivo*) studies did not give a conclusive picture. Indeed, original studies pointed out to ALP impairment in the kidney and lungs of aged LRRK2 KO [25–30] and KD mice [25]. An increase in autophagic markers p62 and LC3-II and a reduction in the lysosomal/endosomal marker LC3-I was found in the optical nerve (for p62 also in striatum and SN) of 15-month-old mice lacking both LRRK1 and LRRK2 that were interpreted as being due to ALP inhibition [31]. Interestingly, however, the same conclusion was reached by studies performed in 15-20-month-old G2019S KI mice [32, 33] or BAC G2019S rats [34] and showing reductions of LC3-I and LAMP1 or increase of LC3-II levels and LC3 puncta in various brain areas. Nonetheless, none of these studies analyzed the autophagic flux *in vivo*, as per accepted recommendations [35], making it difficult to interpret whether the increase observed in LC3-II reflect an increased or decreased autophagic flux.

The current study sought to investigate the role of LRRK2 kinase activity in the modulation of ALP *in vivo*, and how this modulation changes during aging. To this aim, G2019S KI mice (bearing enhanced kinase activity), LRRK2 D1994S KI mice (bearing a kinase-dead mutation; KD mice), LRRK2 knock-out (KO) mice and WT mice were analyzed at 3, 12 and 20 months of age. Western blotting (WB) and RT-qPCR were used to monitor the levels and expression of macroautophagy markers LC3-I, LC3-II, p62, mTOR and its Ser2448 phosphorylated, active form (hereafter referred to as p-mTOR), AMPK and its Thr172 phosphorylated, active form (hereafter referred to as p-AMPK) and CMA markers LAMP2 and GAPDH. The transcript levels of Transcription factor EB (*TFEB*) a master regulator of autophagy and lysosome biogenesis [36, 37] were also measured. Modulation of the autophagic flux *in vivo* was achieved via subacute administration of Chloroquine (CQ), a lysosomotropic agent that inhibits the fusion of autophagosomes with lysosomes [35]. The hydrolytic activity of the lysosomal enzyme Glucocerebrosidase (GCase) was measured in the striatum of 3 and 12-month-old LRRK2 mutant mice. Indeed, impaired GCase activity is associated with PD [38–40] and *GBA1* heterozygous mutations are the

second most common cause of genetic PD [41]. Moreover, the impact of pharmacological inhibition of LRRK2 kinase activity on ALP was investigated via subacute administration of MLi-2. Lastly, to correlate ALP alterations with phosphorylation of α-syn at Serine129 (pSer129 α-syn), an early index of synucleinopathy [42], previously observed in G2019S KI mice [43, 44], co-immunofluorescence analysis was conducted to visualize LC3B puncta and pSer129 α-syn inclusions in striatal MAP+ neurons and nigral TH+ neurons.

Methods

Animals

Experimental procedures involving the use of animals complied with the ARRIVE guidelines and the EU Directive 2010/63/EU for animal experiments and were approved by the Ethical Committee of the University of Ferrara and the Italian Ministry of Health (license 714/2017-PR). Female and male homozygous LRRK2 G2019S KI, KO and KD mice backcrossed for at least 9 generations on a C57BL/6J background, were used [44, 75, 76]. Founders were obtained from Mayo Clinic (Jacksonville, FL, USA) (LRRK2 KO mice) [30] and from Novartis Institutes for BioMedical research (Novartis Pharma AG, Basel, Switzerland) (G2019S KI and KD mice) [25]. A colony of non-transgenic wild-type (WT) mice was initially set from heterozygous breeding of G2019S KI mice, then control WT male mice used in all experiments. Colonies were grown at the *vivarium* (LARP) of the University of Ferrara and kept under regular lighting conditions (12 h light/dark cycle), with free access to food (4RF21 standard diet; Mucedola, Settimo Milanese, Milan, Italy) and water. Animals were housed in groups of 5 for a 55x33x20 cm polycarbonate cage (Tecniplast, Buguggiate, Varese, Italy) with a Scobis Uno bedding (Mucedola, Settimo Milanese, Milan, Italy) and environmental enrichments.

Tissue processing

Mice were anesthetized with isoflurane, transcardially perfused with Phosphate Buffer Solution (PBS), then fixed with 4% paraformaldehyde (PFA) solution (pH 7.4) at 4°C. Brains were dissected out and post-fixed in 4% PFA for 24 h. Brains were then transferred in 30% sucrose in PBS at 4°C and then stored at -80°C. PFA-fixed brains were sectioned at 50 μm (coronal sections) with a cryo-microtome (Leica, Buffalo Grove, Illinois, US) and stored in cryoprotective medium (30% glycerol, 30% ethylene glycol) at -20°C.

LC3B, pSer129 α-syn and MAP2 immunofluorescence

Tissue processing and immunohistochemistry were performed on free-floating sections. Coronal sections of striatum (AP from + 1.0 to -1.25 from bregma) [77] were used for all histological assays. Sections were rinsed 3 times in PBS and blocked in 5% normal goat serum (ab7481, Abcam, Cambridge, Massachusetts, US) and 0.3% TritonX-100 in PBS for 1 h. The following primary antibodies were used: LC3 (1:3000; Rb ab51520, Abcam), pSer129 α-syn (1:2000; Ms ab184674, Abcam), MAP2 (1:1000; Ck ab5392, Abcam), TH (1:1000; Ck ab76442, Abcam). After overnight incubation at 4°C, the primary antibody staining was revealed using donkey anti-Rabbit Secondary Antibody Alexa Fluor 488 (1:1000; A-21206, ThermoFisher

Scientific, Waltham, Massachusetts, US), donkey anti-Mouse Secondary Antibody Alexa Fluor 555 (1:1000; A31570, Thermo Fisher Scientific), goat Anti-Chicken IgY H&L Alexa Fluor 647 (1:1000; ab150171, Abcam). Sections were rinsed in PBS 3 times, incubated in DAPI solution, mounted on Superfrost Plus slides (ThermoFisher Scientific) and coverslipped using antifade Fluoromount G (ThermoFisher Scientific). Images were acquired using a Leica SP8-X confocal microscope at 63X and unbiased estimations of LC3 and pSer129 α-syn in MAP2^{+} and TH^{+} cells were performed (Fiji software, NIH, Bethesda, Maryland, US and Cell Profiler software, Cambridge, Massachusetts, US) by investigators blinded to genotype and experimental conditions.

Western Blot analysis

Mice were anesthetized with isoflurane and sacrificed via cervical dislocation, as described [44, 75, 76]. Striatal tissue was subdissected, snap-frozen and stored at -80°C until further use. Tissue was lysed on ice in 1X RIPA lysis buffer supplemented with 1X Halt protease and phosphatase Inhibitor Cocktail (ThermoFisher Scientific). RIPA lysates were centrifuged at 15,000 g for 10 min at 4°C to remove cellular debris. The pellet was discarded, and clarified lysates were quantified with a Pierce BCA protein assay (ThermoFisher Scientific). Tissue lysates were mixed with 4X LDS Sample buffer, 10X Reducing Agent, equal amounts of protein were subjected to 4−12% Bis-Trisglycine gel or 16% Trisglycine gel and transferred to PVDF membranes (Bio-Rad). Membranes were blocked with 5% milk or 5% BSA in tris-buffered saline with 0.1% Tween (TBST) and immunoblotted according to standard protocols. The following primary antibodies were used for the detection of endogenous LC3 (1:3000; Rb ab51520, Abcam), p62 (1:1000; Rb ab91526, Abcam), LAMP2 (1:1000; Rt ab13524, Abcam), mTOR (1:1000; Rb mAb #2983, CST), phospho-mTOR (Ser2448) (1:1000; Rb mAb #2971, CST), AMPKα (D5A2) (1:1000; Rb BK5831S CST), Phospho-AMPKα (Thr172)(1:1000; Rb mAb BK 2535S CST), phospho-S6K1(Thr389) (1:1000; Rb BK9205S CST), S6K1 (1:1000;Rb BK9202S CST), pSer1292 LRRK2 (1:300; Rb ab203181, Abcam), LRRK2 (1:300; Rb ab133474, Abcam), β-actin (1:3000; Rb ab8227, Abcam). Following incubation at 4°C overnight, horseradish peroxidase-conjugated secondary antibodies, goat anti-Rb (1:4000; 12−348 Merck Millipore, Burlington, Massachusetts, US) and goat anti-Rat (1:4000, AP136P, Merck Millipore), and an ECL kit (ThermoFisher Scientific) were used to detect protein signals. Multiple exposures and images were acquired using the ChemiDoc MP System (Bio-Rad, Hercules, California, US) and protein bands were quantified by densitometry using ImageLab Software (Bio-Rad). β-actin bands were used for normalization.

GCase activity assay

GCase activity was measured as described [78]. Mice were anesthetized with isoflurane and sacrificed via cervical dislocation. Mouse striata (∼15 mg) were dissected out and rapidly homogenized in 150 µl and 250 µl of ice-cold RIPA buffer. Ten micrograms of protein lysates for each sample were diluted in 100 µl of Assay buffer (0.1 M sodium citrate phosphate, pH 5.6; 0.1% Triton X-100; 0.25% sodium taurocholate and 2.5mM 4-4-Methylumbelliferyl β-D-glucopyranoside or 4-MUG). Standard curve (6-point standard curve: 25 µM − 0 µM) was also prepared by serial dilutions of 4-methylumbelliferyl (4-MU, M1381, Sigma-Aldrich, Saint Louis, Missouri, USA) in ddH$_2$0. After incubation with the substrate for 1 h at 37°C, the

reaction was terminated adding 150 µl of stop solution (0.25 M Glycine, pH 10.4). Plates were read (Ex 360/Em 460) in Ensight Perkin Elmer (Perkin-Elmer, Boston, MA, USA), a fluorescent plate reader using Kaleido software (Perkin-Elmer). Enzymatic activity was assessed from a 4-methylumbelliferyl standard curve, whereas protein quantification was determined using a bicinchoninic acid (BCA) assay (ThermoFisher Scientific).

Quantitative Real-Time PCR analysis

Mice were anesthetized with isoflurane and sacrificed via cervical dislocation. Total RNA was extracted from striatal tissue (15 mg) of 12-month-old WT, G2019S KI, KO and KD mice (n = 8 each) using TRI Reagent (Sigma-Aldrich). One microgram of total RNA was treated with DNase I (Thermo Fisher Scientific) and used for cDNA synthesis, performed by the RevertAid First Strand cDNA Synthesis Kit (ThermoFisher Scientific), according to the manufacturer's instructions. Real-time PCR was performed using a CFX Connect Real-time PCR Detection System (Bio-Rad) in 12 µl reaction mixture containing 1.6 µl of 1:5 diluted cDNA, 6 µl SsoAdvanced Universal SYBR Green Supermix (Bio-Rad), 0.4 µl forward primer (10 µM), 0.4 µl reverse primer (10 µM) and 3.6 µl nuclease free water. Thermal cycling condition protocol was set at 95°C for 2 min, 40 cycles at 95°C for 15 s and 60°C for 30 s. After the cycling protocol, a melting-curve analysis from 55°C to 95°C was conducted. Expression of *MAP1LC3*, *TFEB*, *mTOR*, *LAMP2*, *p62*, and *GBA1* genes was normalized using *β-ACT* and *HPRT* as reference genes [79], applying QBase+ method [80]. Gene-specific primers (Table S1) were used, and eight independent biological replicates, made in triplicate, were performed for each genotype.

Drug treatment

CQ, a validated lysosomotropic autophagy inhibitor, was administered (50 mg/kg, i.p.) once daily for three consecutive days to assess the autophagic flux [81]. Mice were anesthetized with isoflurane and sacrificed via cervical dislocation at 4 or 24 h after the last CQ injection and striatal tissues were dissected out to perform WB analysis. To confirm the efficacy of this CQ administration protocol in blocking the autophagolysosomal formation, CQ was first administered to a cohort of 3-month-old WT mice (n = 6). After confirming LC3-II accumulation and the increase of LC3-II/I ratio, the protocol was applied to two cohorts of 12-month-old WT and KD mice (n = 6 each).

MLi-2 treatment

Two cohorts of 12-month-old WT and G2019S KI mice (n = 6 per genotype in each cohort) were subacutely treated with MLi-2 to inhibit LRRK2 kinase activity. Two protocols of MLi-2 administration were adopted: 10 mg/Kg, i.p., twice daily for seven days, or 5 mg/kg, i.p., once daily for seven days. Animals were sacrificed 4 or 12 h after the last injection and one striatum was collected to perform WB analysis, while the other striatum for RT-qPCR analysis.

Drugs

CQ was purchased from Sigma and was dissolved in saline solution. MLi-2 was purchased from Carbosynth (Commpton, Bershire, UK) and was dissolved in 4% DMSO and 30% hydroxyprpyl β-

cyclodextrin.

Statistical analysis

Data are expressed as mean ± SEM (standard error of mean) of n mice. Statistical analysis was performed using Prism 8.0 (GraphPad Software Inc., CA, USA). For experiments with n > 2 groups, one-way ANOVA followed by the Bonferroni's for multiple comparisons was used. QBase + analysis was performed to quantify fold change in gene expression [80], and data analyzed by one-way ANOVA followed by Dunnett's test for multiple comparisons. When only two groups of data were analyzed (e.g., to assess the efficacy of CQ or MLi-2) the Student's t test, two-tailed for unpaired data, was used. Statistical significance was set at $p < 0.05$.

Results

Effect of aging on expression of ALP markers in LRRK2 mice

To evaluate whether age-related dysfunction in striatal macroautophagy and CMA machineries is associated with LRRK2 kinase activity, WB analysis was performed in striatal tissues from 3, 12 and 20-month-old G2019S KI, KO, KD and WT mice. No marker changes across genotypes were observed in 3-month-old mice (Fig. S1). Conversely, changes of LC3-I ($F_{3,28}$=18.03, $p < 0.0001$; Fig. 1A), LC3-II ($F_{3,28}$=2.85, $p = 0.055$, Fig. 1B), p62 ($F_{3,20}$=5.37, $p = 0.0071$), p-mTOR ($F_{3,28}$=12.94, $p < 0.0001$; Fig. 1E), LAMP2 ($F_{3,28}$=8.50, $p = 0.0004$; Fig. 1G) and GAPDH ($F_{3,20}$=11.69, $p = 0.0001$; Fig. 1H) were detected in 12-month-old mice. KD mice showed a ⁓2-fold increase in the abundancy of LC3-I and p62, an 80% elevation of LC3-II and a 72% reduction of p-mTOR with respect to controls. This was associated with an increase of CMA markers LAMP2 (+ 46%) and GAPDH (+ 70%). As far as KO and G2019S KI mice were concerned, a 45% increase of LAMP2 levels was only observed. As AMPK is a functional antagonist of mTOR and promotes autophagy in most systems, AMPK levels were investigated in 12-month-old mice (Fig. S2). AMPK levels were significantly affected across genotypes ($F_{3,20}$=3.62, $p = 0.0308$), being a 50% elevation observed in KD mice.

WB analysis at 20 months (Fig. 2) showed significant changes of LC3-II ($F_{3,20}$=5.49, $p = 0.0065$; Fig. 2B), p62 ($F_{3,20}$=8.53, $p = 0.0008$; Fig. 2D), p-mTOR ($F_{3,20}$=8.91, $p = 0.0006$; Fig. 2E), mTOR ($F_{3,20}$=22.28, $p < 0.0001$; Fig. 2F) and LAMP2 ($F_{3,20}$=4.93, $p = 0.0100$; Fig. 2G) across genotypes. Again, KD mice were most affected, showing increases of LC3-II (+ 30%), p62 (+ 80%) and mTOR (+ 95%) levels along with a 50% reduction of p-mTOR levels. At variance with that observed in younger mice, significant elevations of p62 (+ 47%), mTOR (+ 73%) and LAMP2 (+ 30%) levels were found in KO mice. Conversely, no changes in macroautophagy or CMA markers were observed in G2019S KI mice. To investigate whether the increase of mTOR corresponded to an increase of its activity, the phosphorylation levels of the mTOR substrate, S6K1 were investigated (Fig. S3). No changes in p-S6K1 and S6K1 levels were found (Fig. S3B, C). p-AMPK and AMPK levels were also investigated (Fig. S3D, E). Only p-AMPK levels were significantly

affected across genotypes ($F_{3,20}$=6.93, p = 0.0022). Both KO and KD mice showing marked increases (+ 443% and + 300% respectively), being this effect was just above the limit of significance in KD mice (p = 0.059).

Gene expression analysis of autophagy-related markers at 12 months

To investigate whether changes in protein levels correlated with changes in gene expression, RT-qPCR was performed in striatal extracts from 12-month-old mice (Fig. 3). Changes were observed in mRNA levels of *MAP1LC3B* ($F_{3,28}$=5.23, p = 0.0054; Fig. 3A), *LAMP2* ($F_{3,27}$=13.44, p < 0.0001; Fig. 3C), *mTOR* ($F_{3,28}$=5.39, p = 0.0047; Fig. 3D) and *TFEB* ($F_{3,28}$=3.40, p = 0.0315; Fig. 3E) whereas mRNA levels of *p62* were unaffected (Fig. 3B). KD mice showed a ⬚20% reduction of *mTOR* and *TFEB* mRNA whereas KO mice a 20% reduction of *MAP1LC3B* mRNA. Conversely, G2019S KI mice appeared largely impaired at transcriptional level due to the significant ⬚20% downregulation of *MAP1LC3B*, *LAMP2, TFEB* and *mTOR* gene transcripts.

Autophagic flux assessment in LRRK2 KD mice at 12 months of age

The lysosomotropic autophagy inhibitor CQ was employed to determine whether the LC3 changes were due to increased or impaired ALP [35]. To validate the administration protocol, CQ (50 mg/Kg, i.p.) [45] was administered daily for three consecutive days in 3-month-old WT mice, and animals were sacrificed 24 hours after the last injection (Fig. S4A). A significant ⬚30% increase was found in LC3-II levels (df = 10, t = 2.88, p = 0.0165) and LC3-II/I ratio (df = 10, t = 2.44, p = 0.0350), which is considered an index of effective blockage of autophagosome-lysosome fusion (Fig. S4A) [35]. CQ treatment did not alter the levels of other macroautophagy or CMA markers, such as p62, LAMP2, p-mTOR and mTOR in 3-month-old WT mice (Fig. S4B). The same protocol was then applied to assess the autophagic flux in 12-month-old WT, G2019S KI, KO and KD mice (Fig. S4C). CQ administration significantly reduced the levels of LC3-I (-60%, df = 10, t = 4.20, p = 0.0018), LC3-II (-80%, df = 10, t = 5.70, p = 0.0002) and p62 (-40%, df = 10, t = 3, p = 0.0065) in KD mice (Fig S4C), and elevated LC3-I levels in WT (+ 60%; df = 10, t = 3, p = 0.0107) and G2019S KI (+ 110%; df = 10, t = 3, p = 0.0110) mice (Fig. S4C). However, the LC3-II /I ratio was significantly reduced by ⬚40% in G2019S KI (df = 10, t = 6.11, p = 0.0001), KO (df = 10, t = 5.22, p = 0.0004), KD (df = 10, t = 4.66, p = 0.0009) and WT (df = 10, t = 10, p = 0.0040) mice, suggesting an impairment of the autophagic flux in all genotypes (Fig. S4C). This was accompanied by a consistent elevation of p-mTOR levels across all CQ-treated LRRK2 mutants, that was most dramatic in KD mice: G2019S KI (+ 150%, df = 10, t = 2.55, p = 0.0288), KO mice (+ 110%, df = 10, t = 3.72, p = 0.0040), KD mice (+ 1630%; df = 10, t = 3.74, p = 0.0038). KD mice also showed a 60% reduction of mTOR levels (df = 10, t = 3.41, p = 0.0066). LAMP2 levels were found 57% elevated only in WT mice after CQ treatment (df = 10, t = 3, p = 0.0096; Fig.S4C). These results, in particular the lack of an increase of LC3-II and LC3-II/I ratio in CQ-treated WT mice, led us to hypothesize that these changes were due to a tardive feedback mechanism occurring in all genotypes

as a consequence of the CQ-mediated blockage of the autophagic flux, as previously reported in WT mice [45]. Therefore, CQ administration was replicated anticipating WB analysis at 4 h after the last CQ injection, i.e. when the ALP blockage is still effective. This new administration protocol was performed only in 12-month-old KD mice, i.e. the only genotype showing alterations in LC3-I and LC3-II levels. At this time-point, LC3-I levels were unchanged (Fig. 4A) whereas LC3-II levels (df = 10, t = 5.63, p = 0.0002; Fig. 4B) and the LC3-II/I ratio (df = 10, t = 10.35, p < 0.0001; Fig. 4C) were 2.5-fold elevated in WT mice, likely due to the inhibition of autolysosome formation. Conversely, CQ-treated KD mice exhibited a 30% reduction of LC3-II levels (df = 10, t = 2.31, p = 0.0432) and LC3-II/I ratio (df = 10, t = 2.61, p = 0.0258), indicating a defective autophagic flux (Fig. 4B, C). Consistently, the cargo protein p62 accumulated in CQ-treated WT mice (+ 78%, df = 10, t = 4.30, p = 0.0016) but not in KD mice (Fig. 4D). Conversely, p-mTOR levels were elevated by 2.5-fold in WT mice (df = 10, t = 6.32, p < 0.0001) and by 12-fold in KD mice (df = 10, t = 19.57, p < 0.0001; Fig. 4E) suggesting a marked mTOR activation in both genotypes. This enhancement of mTOR activation was coupled to a 44% reduction in total mTOR levels in KD mice (df = 9, t = 4.18, p = 0.0024; Fig. 4F). LAMP2 levels were elevated by CQ administration in both WT (+ 28%, df = 10, t = 2.60, p = 0.0265) and KD mice (+ 52% df = 10, t = 5.89, p = 0.0002; Fig. 4G).

Changes in GCase activity and GBA1 expression in LRRK2 mice

Since data pointed to a reduced autophagic flux in KD mice, we investigated whether also the activity of lysosomal GCase was affected in LRRK2 mice (Fig. 5). Significant changes were observed both at 3 months ($F_{3,20}$=8.46, p = 0.0008; Fig. 5A) and 12 months ($F_{3,24}$=14.97, p < 0.0001; Fig. 5B). When compared to WT controls, KD mice showed an enhancement at both ages (+ 80% and + 32%, respectively) whereas KO mice only at 12 months (+ 47%), although such increase was significant when the comparison was made against 3-month-old G2019S KI mice (p < 0.05). Conversely, no changes of GCase activity were detected in G2019S KI mice. RT-qPCR analysis interrogated whether changes in GCase activity were accompanied by changes of *GBA1* transcript levels in 12-month-old LRRK2-mutant mice. No significant change in *GBA1* gene expression was detected across genotypes ($F_{3,28}$=2.45, p = 0.0844; Fig. 5C) although a tendency towards a reduction (15%) was observed in G2019S KI mice.

Subacute pharmacological inhibition of LRRK2 kinase activity

To test whether pharmacological LRRK2 kinase inhibition replicates the ALP impairment associated with the constitutive kinase silencing *in vivo*, MLi-2, a potent and brain penetrant LRRK2 kinase inhibitor, was administered subacutely for 7 days in 12-month-old WT and G2019S KI mice. Levels and expression of macroautophagy and CMA markers were evaluated 4 h after the last injection. Target engagement was confirmed by WB analysis of pSer1292 LRRK2 levels, a readout of LRRK2 kinase activity [46], in G2019S KI mice. In a pilot experiment, 10 mg/Kg (i.p.) b.i.d. for 7 days was administered, since this protocol was well tolerated in 3-month-old mice (unpublished data). After a few doses, however, lethality was observed

in some 12-month-old mice of both genotypes prompting us to lower the dosage to 5 mg/Kg (i.p.), once a day for 7 days. Under these conditions, no signs of distress or mortality were noticed. WB analysis revealed a 42% reduction of pSer1292 LRRK2 levels in G2019S KI mice (Fig. S5), indicating effective targeting of LRRK2 *in vivo*. MLi-2 caused a 50% elevation of LC3-I in WT mice (df = 10, t = 2.35, p = 0.00406) but not in G2019S KI mice, and no changes in LC3-II or LC3-II/ I ratio in both genotypes (Fig. 6A). p62 levels were elevated in both WT and G2019S KI mice, although the increase was significant only in G2019S KI mice (+ 80%, df = 10, t = 2.52, p = 0.0303) whereas LAMP2 levels remained unaffected (Fig. 6A). Interestingly, p-mTOR was reduced by ⏷32% (df = 10, t = 2.58, p = 0.00272) and mTOR levels enhanced by ⏷30% (df = 10, t = 2.51, p = 0.0306; Fig. 6A) in G2019S KI mice, whereas no changes were observed in WT mice. RT-qPCR analysis showed that MLi-2 increased *MAP1LC3B* (+ 35%, df = 10, t = 2.62, p = 0.00257), and reduced *mTOR* (-25%, df = 10, t = 3.66, p = 0.0044) and *TFEB* (-20%, df = 10, t = 2.71, p = 0.00218) transcripts in WT mice (Fig. 6B). Moreover, MLi-2 reduced *mTOR* transcripts in G2019S KI mice (-25%, df = 10, t = 3.86, p = 0.0032) and left unaffected *p62* and *LAMP2* transcript levels in both genotypes (Fig. 6B).

Immunofluorescence analysis of LC3B puncta and pSer129 α-syn in striatum and substantia nigra

We previously reported accumulation of pSer129 α-syn soluble forms in the striatum and substantia nigra (SN) of 12-month-old G2019S KI mice [43]. To investigate whether changes in ALP markers were associated with significant increase of neuronal pSer129 α-syn inclusions, immunofluorescence analysis in the striatum and SN of 12-month-old WT, KD, KO and G2019S KI mice was carried out (Fig. 7). Significant changes in LC3 puncta were observed across genotypes ($F_{3,28}$=5.40, p = 0.0046). Consistent with the increase in LC3B-I and LC3B-II detected by WB analysis, LC3B puncta were more abundant (+ 78%) in striatal MAP2$^+$ neurons of KD mice compared to WT mice (Fig. 7A, B) whereas no alterations were observed in KO or G2019S KI mice. On the contrary, pSer129 α-syn signal was elevated in striatal MAP2$^+$ neurons of G2019S KI mice (+ 60%) but not KD and KO mice ($F_{3,28}$=3.68, p = 0.0237) (Fig. 7A, C). LC3B changes were also detected in TH + neurons of SN ($F_{3,29}$=12.47, p < 0.0001), with KD and KO mice showing an increase (2.5-fold and 2-fold, respectively) and G2019S KI mice no change (Fig. 7D, E). However, no changes in pSer129 α-syn signal were observed in TH + neurons across genotypes (Fig. 7F).

Discussion

This study aimed at investigating the role of LRRK2 in the modulation of striatal autophagy and lysosomal function *in vivo*, its kinase- and age-dependence, and relation with pSer129 α-syn inclusions in striatal and nigral neurons, using mice bearing enhanced or silenced LRRK2 kinase activity, or devoid of the full LRRK2 protein. The major finding is that constitutive silencing of LRRK2 kinase activity is associated with deregulation of GCase activity and age-dependent impairment of the autophagic flux.

LRRK2 kinase silencing results in age-dependent inhibition of ALP in vivo

No differences in levels of macroautophagy and CMA markers were observed in the striatum of 3- month-old mice, supporting the hypothesis that no disruption of ALP machinery occurs early in life [47]. Accordingly, no changes in the levels of Akt, mTOR and its substrate TSC2 were observed in the kidneys of 6-week-old G2019S KI, KO and KD mice [25]. Instead, LC3-I and the autophagosome-associated marker LC3-II [48] accumulated in the striatum of 12-month-old KD mice, along with LC3B-I and LC3B-II puncta in both striatal MAP2^{+} and nigral TH^{+} cells. Different lines of experimental evidence support the hypothesis that such changes reflect an impairment and not an upregulation of ALP in striatal neurons of aged mice carrying silenced LRRK2 kinase activity. First, CQ prevents lysosomal acidification causing blockage of autophagolysosome formation, and if ALP were normally active or even upregulated, an increase of LC3-II/I ratio would be expected after CQ administration [45], as indeed observed in WT mice. The reduction of LC3-II/I ratio, instead, indicates that CQ caused a further blockage of an already compromised autolysosome fusion step. Second, the selective autophagy receptor and autophagic clearance marker p62 accumulated in KD mice. Moreover, p62 levels were elevated in WT mice but unchanged in KD mice after CQ treatment. Third, the levels of *MAP1LC3B* and *p62* transcripts were unchanged in KD mice, suggesting that the increase of LC3-I, LC3-II and p62 protein levels was not associated with an increased synthesis, as it might be expected if autophagic flux were up-regulated. Moreover, *TFEB*, a promoter of autophagy and lysosome biogenesis [36, 37] was downregulated in KD mice.

If ALP is impaired in KD mice, the reduction of mTOR phosphorylated (i.e. active) form might reflect a compensatory mechanism to sustain a defective autophagic flux, since it is a negative regulator of ALP [49]. This is also supported by the concurrent increase of AMPK levels in KD mice since AMPK and mTOR oppositely regulate the activity of the autophagy initiator ULK1 [49]. The dramatic increase of p-mTOR levels in both WT and KD mice following CQ might thus reflect a general feedback mechanism aimed to inhibit ALP following lysosomal stress [50]. Nonetheless, a similar reduction of p-mTOR in 20-month-old KD mice was not associated with a reduction of the phosphorylation of its substrate pS6K1. Although we did not measure the phosphorylation levels of another mTOR substrate EIF4EBP1 and, therefore, we cannot rule out the possibility of a differential regulation, the present data would suggest that changes in mTOR phosphorylation do not translate in changes of mTOR activity. Thus, as pointed out by different *in vitro* [51, 52] and *in vivo* [25] studies it is possible that LRRK2 modulation of ALP occurs independently of mTOR, since mTOR is at the crossroad of signaling pathways involved in cellular survival, metabolism and homeostasis [53].

CMA also is likely inhibited in 12-month-old KD mice. In fact, the levels of both the lysosomal receptor LAMP2 and the CMA substrate GAPDH are elevated under basal conditions (each measure alone would not allow to draw any conclusion on CMA activity) [54, 55] whereas *LAMP2* transcript levels were unchanged. These data point to lysosomal accumulation and impaired GAPDH clearance in striatum.

The finding that CQ increased the striatal levels of LAMP2 in both WT and KD mice would confirm that blockade of autophagosome formation causes lysosomal overload.

At 20 months, KD mice still showed an accumulation of the macroautophagy markers LC3-II and p62, possibly confirming a long-lasting ALP impairment. This was coupled to a reduced phosphorylation of p-mTOR but not of its substrate pS6K1, and an increase of the phosphorylated, active form of AMPK. LAMP2 and GAPDH were unchanged at this age, suggesting normalization of CMA activity. It is noteworthy that mild changes in ALP markers similar to those observed in KD mice, i.e. elevated p62 and mTOR levels associated with a slight reduction of p-mTOR levels, became evident in 20-month-old KO mice, suggesting a late ALP dysregulation also in mice devoid of LRRK2. This is in contrast with the lack of changes of ALP markers reported in the brain of 15-month-old LRRK2 KO mice [31], although the different age at analysis might explain the inconsistency. Nonetheless, our data are in line with the striking age-dependent ALP and lysosomal impairment associated with kidney pathology, consistently reported in LRRK2 KO rodents *in vivo* [25–30]. The kidney pathology in KO mice, however, is characterized by an earlier onset and more severe course compared to the brain pathology. This might be due to the greater levels of LRRK2 expression in the kidney or to a LRRK1 compensatory role in the brain [31]. In fact, LRRK1 regulates autophagy in cooperation with LRRK2 [56]. LAMP2 levels were also significantly elevated in 20-month-old KO mice, although this was not associated with changes in GAPDH protein levels or *LAMP2* gene expression, making it impossible to draw any conclusion on the CMA status in these animals. In contrast with the reduction of LC3-I and LAMP1 levels found in the cerebral cortex of 20-month-old G2019S KI mice [32] macroautophagy markers were unchanged in the striatum of G2019S KI mice, in line with that found in the basal ganglia of G2019S PD patients [57]. G2019S KI mice showed an increase of LAMP2 (but not GAPDH) levels at 12 months which is in partial agreement with the increase of striatal LAMP2 and GAPDH levels in aged R1441G KI mice that was proposed to reflect CMA impairment [58]. The inconsistence of the GAPDH changes in the two studies might be related to the different LRRK2 mutation [34]. Nonetheless, significant downregulation of *MAP1LC3B*, *LAMP2*, *mTOR* and *TFEB* was observed in the striatum of 12-month-old G2019S KI mice possibly suggesting a defective transcription associated with compensatory post-translational regulation.

LRRK2 inhibits GCase activity in vivo through its kinase function

Consistent with the enhanced GCase hydrolytic activity in LRRK2 KO astrocytes [59], the present study found elevated striatal GCase activity in LRRK2 KO and KD mice *in vivo*, indicating that striatal GCase activity is negatively regulated by LRRK2 kinase. Indeed, MLi-2 rescued the impairment of GCase activity in G2019S patient-derived fibroblasts and DA neurons [60]. According to this study, the increased enzymatic activity observed in both LRRK2 kinase-absent genotypes was not associated with changes of *GBA1* transcript, possibly suggesting a defective intracellular trafficking of GCase [60]. The lack of GCase changes in the striatum of G2019S KI mice (only a trend towards an inhibition was observed) might indicate that the inhibitory regulation is already maximal under physiological conditions so further increase of LRRK2 kinase activity associated with the G2019S mutation does not cause additional

inhibition. Nonetheless, the mild reduction of *GBA1* expression observed in 12-month-old G2019S KI mice is consistent with that found in the human PD brain [40]. Elevated GCase activity was observed in 3-month-old and 12-month-old mice, suggesting that changes in lysosomal function precede changes of ALP markers observed in these genotypes.

Pharmacological inhibition of LRRK2 kinase activity

To investigate the impact of LRRK2 kinase inhibition on ALP under conditions of normal and enhanced kinase activity, subacute MLi-2 was administered in 12-month-old WT and G2019S KI mice. Aged mice were exquisitely sensitive to MLi-2 irrespective of genotype, since they did not tolerate high MLi-2 dosage causing profound inhibition of kinase activity (pSer1292 levels were reduced by ⁓80% in surviving G2019S KI mice, not shown). Under a safe MLi-2 dosage (associated with 42% reduction of striatal pSer1292 LRRK2), an increase of LC3-I levels and *MAP1LC3B* expression was observed in WT mice. G2019S KI mice were more affected showing an increase of p62 and mTOR and a reduction of p-mTOR levels along with a reduction of *mTOR* expression. In any genotype, subacute MLi-2 administration replicated the phenotype of 12-month-old KD mice, possibly due to adaptation phenomena accompanying constitutive silencing of LRRK2 kinase activity and/or the mild level of LRRK2 kinase inhibition achieved with the subacute protocol.

Various *in vitro* studies reported that LRRK2 kinase inhibitors, among which MLi-2, improve the autophagic flux or rescue the lysosomal defects associated with G2019S LRRK2 [32, 34, 51, 61–63] whereas other showed the opposite [64]. Our data cannot either support or confute this view, considering that elevation of p62 (not associated with changes of *p62* transcript) and reduction of *TFEB* transcript point to ALP blockade while the increase of LC3-I levels and expression suggest the opposite. Although sub-acute inhibition of LRRK2 kinase activity did not recapitulate the ALP deficits measured in 12-month-old KD mice, it can provide information on ALP targets regulated by endogenous LRRK2 control and, therefore, more sensitive to LRRK2 kinase inhibition. Indeed, the enhancement of LRRK2 kinase activity in G2019S KI mice brings mTOR function under a stronger LRRK2 control. LRRK2 inhibitors are currently under investigation as disease modifying agents in PD [65]. Although our data cannot tell whether the MLi-2 toxicity observed in aged mice is LRRK2-related, they nonetheless confirm that dosage of LRRK2 inhibitors need to be carefully titrated in aged subjects to avoid profound inhibition of LRRK2 kinase function [65]. Moreover, further studies are needed to ascertain the effects of long-term treatment with LRRK2 inhibitors on ALP function, particularly in aged animals.

Relationship between ALP impairment and pSer129 α-syn inclusions

Previous *in vivo* studies have shown α-syn oligomer appearance to be associated with CMA impairment in 18-month-old R1441G LRRK2 mice [58] or with autophagy impairment in 15-month-old LRRK double KO mice [31] suggesting a link between ALP impairment and synucleinopathy. pSer129 α-syn inclusions can be viewed as an early index of synucleinopathy [42] since Ser129 phosphorylation increases the propensity of α-syn to aggregate and propagate [66]. Moreover, pSer129 α-syn co-stains with markers of

Lewy body pathology in models of PD progression [67, 68] and is highly enriched in Lewy Bodies [69, 70]. Based on previous findings that G2019S LRRK2 facilitated α-syn phosphorylation at Ser129 and nigrostriatal neurodegeneration [43, 71], the possibility that pSer129 α-syn inclusions were associated with ALP impairment was considered. We previously observed the development of soluble pSer129 α-syn inclusions in the striatum and SNc of G2019S KI mice during aging [43, 44]. Here, we localize pSer129 α-syn inclusions in striatal MAP2^{+} neurons, very likely GABAergic neurons since they represent by far (> 95%) the most abundant striatal cell population [72]. In line with WB data, however, striatal G2019S neurons did not show altered LC3B puncta levels whereas striatal LRRK2 KD neurons showed increase in LC3B puncta but not in pSer129 α-syn inclusions. Thus, ALP impairment and pSer129 α-syn inclusions occur in different neuronal types. Based on this finding, we should conclude that the greater nigrostriatal degeneration observed in aged G2019S KI mice following virally-induced α-syn overload is due to neuronal ALP-independent mechanisms. However, there might not be a relation between pSer129 α-syn inclusions observed under basal conditions in G2019S KI mice and their enhanced susceptibility to parkinsonism. Indeed, a recent study showed that presynaptic pools of neuronal pSer129 α-syn exist that are unrelated to Lewy Body pathology [73]. This would suggest that striatal pSer129 α-syn inclusions observed in aged G2019S KI mice under basal conditions might have some bearing with the neuronal dysfunctions observed in these mice [44]. On the other hand, it cannot be ruled out that the ALP impairment in KO mice also facilitates synucleinopathy in the presence of α-syn overload, due to the expected defective α-syn handling.

Conclusions

This study provides strong evidence that constitutive silencing of LRRK2 kinase activity results in early deregulation of GCase activity and late impairment of macroautophagy and CMA, whereas genetic deletion of LRRK2 is associated with early deregulation of GCase activity followed by an even more delayed ALP pattern reminiscent of ALP impairment, possibly indicating a contribution of LRRK2 scaffolding properties and GTPase activity or simply the loss of LRRK1 compensation. Expression of pathogenic G2019S mutation was not accompanied by changes of striatal macroautophagy markers but downregulation of key autophagy and lysosomal genes, as reported in the PD brain [74]. This might indicate that striatal ALP changes are unlike to contribute to G2019S synucleinopathy. This study contributes to shed light into the complex modulation exerted by LRRK2 over ALP *in vivo*, demonstrating that LRRK2 kinase activity is essential for a proper ALP function during aging.

Abbreviations

ALP Autophagy-lysosomal pathway

CMA Chaperone-mediated autophagy

CQ Chloroquine

GCase Glucocerebrosidase

KD Kinase-dead

KI Knock-in

KO Knock-out

LRRK1 Leucine-rich repeat kinase 1

LRRK2 Leucine-rich repeat kinase 2

α-syn α-synuclein

PD Parkinson's disease

pSer129 α-syn phosphoSerine 129 α-synuclein

pSer1292 LRRK2 phosphoSerine 1292 LRRK2

TFEB Transcription factor EB

WT Wild-type

Declarations

Ethical approval and consent to participate

Experimental procedures involving the use of animals were approved by the Ethical Committee of the University of Ferrara and the Italian Ministry of Health (license 714/2017-PR).

Consent for publication

Not applicable

Availability of supporting data

The datasets generated during and/or analyzed during the current study are available from the corresponding author on reasonable request

Competing interests

DRS is an employee of Novartis Pharma AG. The other authors report no competing financial interests.

Funding

Authors' information

Affiliations

Department of Neuroscience and Rehabilitation, Section of Pharmacology, University of Ferrara,44121 Ferrara, Italy.

Federica Albanese, Daniela Mercatelli, Michele Morari

D.M. Technopole of Ferrara, LTTA Laboratory for Advanced Therapies, 44121 Ferrara, Italy

Daniela Mercatelli

Department of Life Sciences and Biotechnology, University of Ferrara, 44121 Ferrara, Italy

Luca Finetti, Giovanni Bernacchia

 Institute for Biomedicine, Eurac Research-Affiliated Institute of the University of Lübeck, 39100 Bolzano, Italy

Giulia Lamonaca, Sara Pizzi

Department of Neuroscience, Novartis Institutes for BioMedical Research, Novartis Pharma AG, 4002 Basel, Switzerland

Derya Shimshek

Corresponding Author

Michele Morari

References

1. Poewe W, Seppi K, Tanner CM, Halliday GM, Brundin P, Volkmann J, Schrag AE, Lang AE. Parkinson disease. Nature reviews Disease primers. 2017;3:17013.

2. Kluss JH, Mamais A, Cookson MR. LRRK2 links genetic and sporadic Parkinson's disease. Biochem Soc Trans. 2019;47:651–61.

3. Cookson MR. Mechanisms of Mutant LRRK2 Neurodegeneration. Advances in neurobiology. 2017;14:227–39.

4. Cookson MR. The role of leucine-rich repeat kinase 2 (LRRK2) in Parkinson's disease. Nat Rev Neurosci. 2010;11:791–7.

5. Mata IF, Wedemeyer WJ, Farrer MJ, Taylor JP, Gallo KA. LRRK2 in Parkinson's disease: protein domains and functional insights. Trends Neurosci. 2006;29:286–93.

6. Nalls MA, Pankratz N, Lill CM, Do CB, Hernandez DG, Saad M, DeStefano AL, Kara E, Bras J, Sharma M, et al. Large-scale meta-analysis of genome-wide association data identifies six new risk loci for Parkinson's disease. Nat Genet. 2014;46:989–93.

7. Berwick DC, Heaton GR, Azeggagh S, Harvey K. LRRK2 Biology from structure to dysfunction: research progresses, but the themes remain the same. Mol Neurodegener. 2019;14:49.

8. West AB, Moore DJ, Biskup S, Bugayenko A, Smith WW, Ross CA, Dawson VL, Dawson TM. Parkinson's disease-associated mutations in leucine-rich repeat kinase 2 augment kinase activity. Proc Natl Acad Sci U S A. 2005;102:16842–7.

9. Greggio E, Jain S, Kingsbury A, Bandopadhyay R, Lewis P, Kaganovich A, van der Brug MP, Beilina A, Blackinton J, Thomas KJ, et al. Kinase activity is required for the toxic effects of mutant LRRK2/dardarin. Neurobiol Dis. 2006;23:329–41.

10. Yao C, El Khoury R, Wang W, Byrd TA, Pehek EA, Thacker C, Zhu X, Smith MA, Wilson-Delfosse AL, Chen SG. LRRK2-mediated neurodegeneration and dysfunction of dopaminergic neurons in a Caenorhabditis elegans model of Parkinson's disease. Neurobiol Dis. 2010;40:73–81.

11. Heo HY, Park JM, Kim CH, Han BS, Kim KS, Seol W. LRRK2 enhances oxidative stress-induced neurotoxicity via its kinase activity. Exp Cell Res. 2010;316:649–56.

12. Smith WW, Pei Z, Jiang H, Dawson VL, Dawson TM, Ross CA. Kinase activity of mutant LRRK2 mediates neuronal toxicity. Nat Neurosci. 2006;9:1231–3.

13. Plowey ED, Chu CT. Synaptic dysfunction in genetic models of Parkinson's disease: a role for autophagy? Neurobiol Dis. 2011;43:60–7.

14. Albanese F, Novello S, Morari M. Autophagy and LRRK2 in the Aging Brain. Front NeuroSci. 2019;13:1352.

15. Manzoni C, Lewis PA. LRRK2 and Autophagy. Advances in neurobiology. 2017;14:89–105.

16. Gan-Or Z, Dion PA, Rouleau GA. Genetic perspective on the role of the autophagy-lysosome pathway in Parkinson disease. Autophagy. 2015;11:1443–57.

17. Tsika E, Moore DJ. Mechanisms of LRRK2-mediated neurodegeneration. Curr Neurol Neurosci Rep. 2012;12:251–60.

18. Galluzzi L, Bravo-San Pedro JM, Levine B, Green DR, Kroemer G. Pharmacological modulation of autophagy: therapeutic potential and persisting obstacles. Nat Rev Drug Discov. 2017;16:487–511.

19. Boland B, Yu WH, Corti O, Mollereau B, Henriques A, Bezard E, Pastores GM, Rubinsztein DC, Nixon RA, Duchen MR, et al. Promoting the clearance of neurotoxic proteins in neurodegenerative disorders of ageing. Nat Rev Drug Discov. 2018;17:660–88.

20. Cuervo AM. Autophagy and aging: keeping that old broom working. Trends Genet. 2008;24:604–12.

21. Xilouri M, Vogiatzi T, Vekrellis K, Stefanis L. alpha-synuclein degradation by autophagic pathways: a potential key to Parkinson's disease pathogenesis. Autophagy. 2008;4:917–9.

22. Johnson ME, Stecher B, Labrie V, Brundin L, Brundin P. Triggers, Facilitators, and Aggravators: Redefining Parkinson's Disease Pathogenesis. Trends Neurosci. 2019;42:4–13.

23. Madureira M, Connor-Robson N, Wade-Martins R. "LRRK2: Autophagy and Lysosomal Activity". Front NeuroSci. 2020;14:498.

24. Senkevich K, Gan-Or Z. Autophagy lysosomal pathway dysfunction in Parkinson's disease; evidence from human genetics. Parkinsonism Relat Disord. 2020;73:60–71.

25. Herzig MC, Kolly C, Persohn E, Theil D, Schweizer T, Hafner T, Stemmelen C, Troxler TJ, Schmid P, Danner S, et al. LRRK2 protein levels are determined by kinase function and are crucial for kidney and lung homeostasis in mice. Hum Mol Genet. 2011;20:4209–23.

26. Fuji RN, Flagella M, Baca M, Baptista MA, Brodbeck J, Chan BK, Fiske BK, Honigberg L, Jubb AM, Katavolos P, et al. Effect of selective LRRK2 kinase inhibition on nonhuman primate lung. Sci Transl Med. 2015;7:273ra215.

27. Tong Y, Yamaguchi H, Giaime E, Boyle S, Kopan R, Kelleher RJ 3rd, Shen J. Loss of leucine-rich repeat kinase 2 causes impairment of protein degradation pathways, accumulation of alpha-synuclein, and apoptotic cell death in aged mice. Proc Natl Acad Sci U S A. 2010;107:9879–84.

28. Tong Y, Giaime E, Yamaguchi H, Ichimura T, Liu Y, Si H, Cai H, Bonventre JV, Shen J. Loss of leucine-rich repeat kinase 2 causes age-dependent bi-phasic alterations of the autophagy pathway. Mol Neurodegener. 2012;7:2.

29. Baptista MA, Dave KD, Frasier MA, Sherer TB, Greeley M, Beck MJ, Varsho JS, Parker GA, Moore C, Churchill MJ, et al. Loss of leucine-rich repeat kinase 2 (LRRK2) in rats leads to progressive abnormal phenotypes in peripheral organs. PLoS One. 2013;8:e80705.

30. Hinkle KM, Yue M, Behrouz B, Dachsel JC, Lincoln SJ, Bowles EE, Beevers JE, Dugger B, Winner B, Prots I, et al. LRRK2 knockout mice have an intact dopaminergic system but display alterations in exploratory and motor co-ordination behaviors. Mol Neurodegener. 2012;7:25.

31. Giaime E, Tong Y, Wagner LK, Yuan Y, Huang G, Shen J. Age-Dependent Dopaminergic Neurodegeneration and Impairment of the Autophagy-Lysosomal Pathway in LRRK-Deficient Mice. Neuron. 2017;96:796–807 e796.

32. Schapansky J, Khasnavis S, DeAndrade MP, Nardozzi JD, Falkson SR, Boyd JD, Sanderson JB, Bartels T, Melrose HL, LaVoie MJ. Familial knockin mutation of LRRK2 causes lysosomal dysfunction and accumulation of endogenous insoluble alpha-synuclein in neurons. Neurobiol Dis. 2018;111:26−35.

33. Yue M, Hinkle KM, Davies P, Trushina E, Fiesel FC, Christenson TA, Schroeder AS, Zhang L, Bowles E, Behrouz B, et al. Progressive dopaminergic alterations and mitochondrial abnormalities in LRRK2 G2019S knock-in mice. Neurobiol Dis. 2015;78:172−95.

34. Wallings R, Connor-Robson N, Wade-Martins R. LRRK2 interacts with the vacuolar-type H+-ATPase pump a1 subunit to regulate lysosomal function. Hum Mol Genet. 2019;28:2696−710.

35. Klionsky DJ, Abdel-Aziz AK, Abdelfatah S, Abdellatif M, Abdoli A, Abel S, Abeliovich H, Abildgaard MH, Abudu YP, Acevedo-Arozena A, et al: Guidelines for the use and interpretation of assays for monitoring autophagy (4th edition)(1). *Autophagy* 2021, **17**:1-382.

36. Sardiello M, Palmieri M, di Ronza A, Medina DL, Valenza M, Gennarino VA, Di Malta C, Donaudy F, Embrione V, Polishchuk RS, et al. A gene network regulating lysosomal biogenesis and function. Science. 2009;325:473−7.

37. Settembre C, Fraldi A, Medina DL, Ballabio A. Signals from the lysosome: a control centre for cellular clearance and energy metabolism. Nature reviews Molecular cell biology. 2013;14:283−96.

38. Chiasserini D, Paciotti S, Eusebi P, Persichetti E, Tasegian A, Kurzawa-Akanbi M, Chinnery PF, Morris CM, Calabresi P, Parnetti L, Beccari T. Selective loss of glucocerebrosidase activity in sporadic Parkinson's disease and dementia with Lewy bodies. Mol Neurodegener. 2015;10:15.

39. Gegg ME, Burke D, Heales SJ, Cooper JM, Hardy J, Wood NW, Schapira AH. Glucocerebrosidase deficiency in substantia nigra of parkinson disease brains. Ann Neurol. 2012;72:455−63.

40. Murphy KE, Gysbers AM, Abbott SK, Tayebi N, Kim WS, Sidransky E, Cooper A, Garner B, Halliday GM. Reduced glucocerebrosidase is associated with increased alpha-synuclein in sporadic Parkinson's disease. Brain. 2014;137:834−48.

41. Sidransky E, Samaddar T, Tayebi N: **Mutations in GBA are associated with familial Parkinson disease susceptibility and age at onset**. *Neurology* 2009, **73**:1424−1425, author reply 1425−1426.

42. Oueslati A. Implication of Alpha-Synuclein Phosphorylation at S129 in Synucleinopathies: What Have We Learned in the Last Decade? Journal of Parkinson's disease. 2016;6:39−51.

43. Novello S, Arcuri L, Dovero S, Dutheil N, Shimshek DR, Bezard E, Morari M. G2019S LRRK2 mutation facilitates alpha-synuclein neuropathology in aged mice. Neurobiol Dis. 2018;120:21−33.

44. Longo F, Mercatelli D, Novello S, Arcuri L, Brugnoli A, Vincenzi F, Russo I, Berti G, Mabrouk OS, Kennedy RT, et al. Age-dependent dopamine transporter dysfunction and Serine129 phospho-alpha-synuclein overload in G2019S LRRK2 mice. Acta neuropathologica communications. 2017;5:22.

45. Vodicka P, Lim J, Williams DT, Kegel KB, Chase K, Park H, Marchionini D, Wilkinson S, Mead T, Birch H, et al. Assessment of chloroquine treatment for modulating autophagy flux in brain of WT and HD mice. Journal of Huntington's disease. 2014;3:159−74.

46. Kluss JH, Conti MM, Kaganovich A, Beilina A, Melrose HL, Cookson MR, Mamais A. Detection of endogenous S1292 LRRK2 autophosphorylation in mouse tissue as a readout for kinase activity. NPJ Parkinson's disease. 2018;4:13.

47. Rubinsztein DC, Marino G, Kroemer G. Autophagy and aging. Cell. 2011;146:682–95.

48. Mizushima N, Yoshimori T, Levine B. Methods in mammalian autophagy research. Cell. 2010;140:313–26.

49. Kim J, Kundu M, Viollet B, Guan KL. AMPK and mTOR regulate autophagy through direct phosphorylation of Ulk1. Nat Cell Biol. 2011;13:132–41.

50. Wang B, Zhong Y, Li Q, Cui L, Huang G. Autophagy of macrophages is regulated by PI3k/Akt/mTOR signalling in the development of diabetic encephalopathy. Aging. 2018;10:2772–82.

51. Manzoni C, Mamais A, Dihanich S, Abeti R, Soutar MPM, Plun-Favreau H, Giunti P, Tooze SA, Bandopadhyay R, Lewis PA. Inhibition of LRRK2 kinase activity stimulates macroautophagy. Biochim Biophys Acta. 2013;1833:2900–10.

52. Manzoni C, Mamais A, Dihanich S, Soutar MPM, Plun-Favreau H, Bandopadhyay R, Abeti R, Giunti P, Hardy J, M RC, et al: **mTOR independent alteration in ULK1 Ser758 phosphorylation following chronic LRRK2 kinase inhibition**. *Bioscience reports* 2018, 38.

53. Liu GY, Sabatini DM. mTOR at the nexus of nutrition, growth, ageing and disease. Nature reviews Molecular cell biology. 2020;21:183–203.

54. Kaushik S, Cuervo AM. Chaperone-mediated autophagy: a unique way to enter the lysosome world. Trends in cell biology. 2012;22:407–17.

55. Cuervo AM, Stefanis L, Fredenburg R, Lansbury PT, Sulzer D. Impaired degradation of mutant alpha-synuclein by chaperone-mediated autophagy. Science. 2004;305:1292–5.

56. Toyofuku T, Morimoto K, Sasawatari S, Kumanogoh A. Leucine-Rich Repeat Kinase 1 Regulates Autophagy through Turning On TBC1D2-Dependent Rab7 Inactivation. Mol Cell Biol. 2015;35:3044–58.

57. Mamais A, Manzoni C, Nazish I, Arber C, Sonustun B, Wray S, Warner TT, Cookson MR, Lewis PA, Bandopadhyay R. Analysis of macroautophagy related proteins in G2019S LRRK2 Parkinson's disease brains with Lewy body pathology. Brain Res. 2018;1701:75–84.

58. Ho PW, Leung CT, Liu H, Pang SY, Lam CS, Xian J, Li L, Kung MH, Ramsden DB, Ho SL. Age-dependent accumulation of oligomeric SNCA/alpha-synuclein from impaired degradation in mutant LRRK2 knockin mouse model of Parkinson disease: role for therapeutic activation of chaperone-mediated autophagy (CMA). Autophagy. 2020;16:347–70.

59. Ferrazza R, Cogo S, Melrose H, Bubacco L, Greggio E, Guella G, Civiero L, Plotegher N. LRRK2 deficiency impacts ceramide metabolism in brain. Biochem Biophys Res Commun. 2016;478:1141–6.

60. Ysselstein D, Nguyen M, Young TJ, Severino A, Schwake M, Merchant K, Krainc D. LRRK2 kinase activity regulates lysosomal glucocerebrosidase in neurons derived from Parkinson's disease patients. Nature communications. 2019;10:5570.

61. Obergasteiger J, Frapporti G, Lamonaca G, Pizzi S, Picard A, Lavdas AA, Pischedda F, Piccoli G, Hilfiker S, Lobbestael E, et al. Kinase inhibition of G2019S-LRRK2 enhances autolysosome formation and function to reduce endogenous alpha-synuclein intracellular inclusions. Cell death discovery. 2020;6:45.

62. Boecker CA, Goldsmith J, Dou D, Cajka GG, Holzbaur ELF. **Increased LRRK2 kinase activity alters neuronal autophagy by disrupting the axonal transport of autophagosomes**. *Curr Biol* 2021.

63. Saez-Atienzar S, Bonet-Ponce L, Blesa JR, Romero FJ, Murphy MP, Jordan J, Galindo MF. The LRRK2 inhibitor GSK2578215A induces protective autophagy in SH-SY5Y cells: involvement of Drp-1-mediated mitochondrial fission and mitochondrial-derived ROS signaling. Cell death disease. 2014;5:e1368.

64. Schapansky J, Nardozzi JD, Felizia F, LaVoie MJ. Membrane recruitment of endogenous LRRK2 precedes its potent regulation of autophagy. Hum Mol Genet. 2014;23:4201–14.

65. Tolosa E, Vila M, Klein C, Rascol O. LRRK2 in Parkinson disease: challenges of clinical trials. Nat Rev Neurol. 2020;16:97–107.

66. Samuel F, Flavin WP, Iqbal S, Pacelli C, Sri Renganathan SD, Trudeau LE, Campbell EM, Fraser PE, Tandon A. Effects of Serine 129 Phosphorylation on alpha-Synuclein Aggregation, Membrane Association, and Internalization. J Biol Chem. 2016;291:4374–85.

67. Niu H, Shen L, Li T, Ren C, Ding S, Wang L, Zhang Z, Liu X, Zhang Q, Geng D, et al. Alpha-synuclein overexpression in the olfactory bulb initiates prodromal symptoms and pathology of Parkinson's disease. Translational neurodegeneration. 2018;7:25.

68. Luk KC, Kehm V, Carroll J, Zhang B, O'Brien P, Trojanowski JQ, Lee VM. Pathological alpha-synuclein transmission initiates Parkinson-like neurodegeneration in nontransgenic mice. Science. 2012;338:949–53.

69. Fujiwara H, Hasegawa M, Dohmae N, Kawashima A, Masliah E, Goldberg MS, Shen J, Takio K, Iwatsubo T. alpha-Synuclein is phosphorylated in synucleinopathy lesions. Nat Cell Biol. 2002;4:160–4.

70. Anderson JP, Walker DE, Goldstein JM, de Laat R, Banducci K, Caccavello RJ, Barbour R, Huang J, Kling K, Lee M, et al. Phosphorylation of Ser-129 is the dominant pathological modification of alpha-synuclein in familial and sporadic Lewy body disease. J Biol Chem. 2006;281:29739–52.

71. Volpicelli-Daley LA, Abdelmotilib H, Liu Z, Stoyka L, Daher JP, Milnerwood AJ, Unni VK, Hirst WD, Yue Z, Zhao HT, et al. G2019S-LRRK2 Expression Augments alpha-Synuclein Sequestration into Inclusions in Neurons. J Neurosci. 2016;36:7415–27.

72. Gerfen CR. The neostriatal mosaic: multiple levels of compartmental organization. Trends Neurosci. 1992;15:133–9.

73. Weston LJ, Stackhouse TL, Spinelli KJ, Boutros SW, Rose EP, Osterberg VR, Luk KC, Raber J, Weissman TA, Unni VK. **Genetic deletion of Polo-like kinase 2 reduces alpha-synuclein serine-129 phosphorylation in presynaptic terminals but not Lewy bodies**. *J Biol Chem* 2021:100273.

74. Decressac M, Mattsson B, Weikop P, Lundblad M, Jakobsson J, Bjorklund A. TFEB-mediated autophagy rescues midbrain dopamine neurons from alpha-synuclein toxicity. Proc Natl Acad Sci U S A. 2013;110:E1817–26.

75. Longo F, Russo I, Shimshek DR, Greggio E, Morari M. Genetic and pharmacological evidence that G2019S LRRK2 confers a hyperkinetic phenotype, resistant to motor decline associated with aging. Neurobiol Dis. 2014;71:62–73.

76. Mercatelli D, Bolognesi P, Frassineti M, Pisano CA, Longo F, Shimshek DR, Morari M. Leucine-rich repeat kinase 2 (LRRK2) inhibitors differentially modulate glutamate release and Serine935 LRRK2 phosphorylation in striatal and cerebrocortical synaptosomes. Pharmacol Res Perspect. 2019;7:e00484.

77. Paxinos G, Franklin KBJ. The mouse brain in stereotaxic coordinates. 2nd ed. San Diego: Academic Press; 2001.

78. Ambrosi G, Ghezzi C, Zangaglia R, Levandis G, Pacchetti C, Blandini F. Ambroxol-induced rescue of defective glucocerebrosidase is associated with increased LIMP-2 and saposin C levels in GBA1 mutant Parkinson's disease cells. Neurobiol Dis. 2015;82:235–42.

79. Gong H, Sun L, Chen B, Han Y, Pang J, Wu W, Qi R, Zhang TM. Evaluation of candidate reference genes for RT-qPCR studies in three metabolism related tissues of mice after caloric restriction. Sci Rep. 2016;6:38513.

80. Hellemans J, Mortier G, De Paepe A, Speleman F, Vandesompele J. qBase relative quantification framework and software for management and automated analysis of real-time quantitative PCR data. Genome biology. 2007;8:R19.

81. Mauthe M, Orhon I, Rocchi C, Zhou X, Luhr M, Hijlkema KJ, Coppes RP, Engedal N, Mari M, Reggiori F. Chloroquine inhibits autophagic flux by decreasing autophagosome-lysosome fusion. Autophagy. 2018;14:1435–55.

Figures
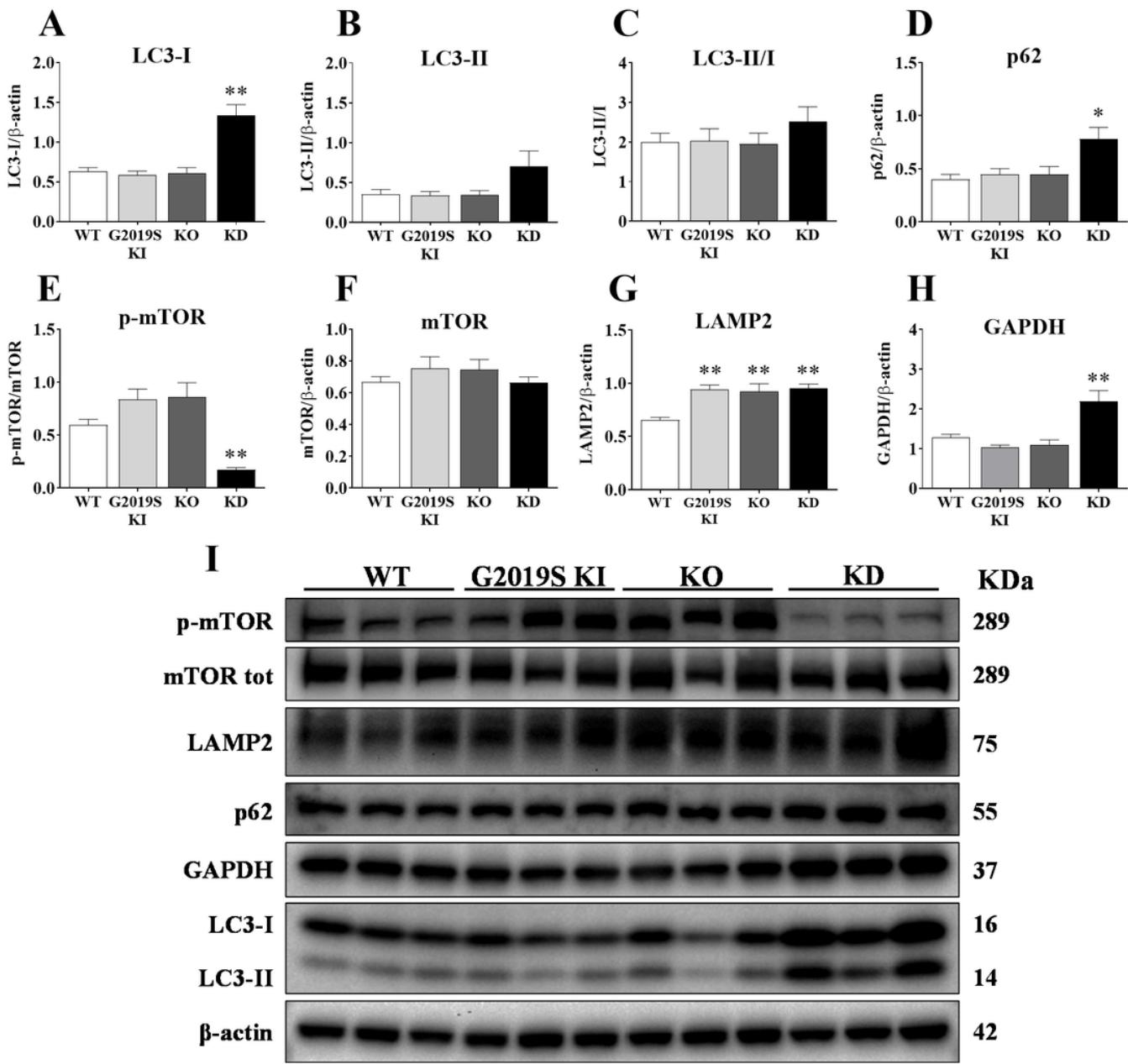
Figure 1

Immunoblot analysis of autophagy-lysosomal pathway (ALP) markers in 12-month-old LRRK2 mice. Striatum lysates from 12-month-old WT, G2019S KI, KO and KD mice. Semi-quantitative analysis of macroautophagy markers levels: LC3-I (A), LC3-II (B), LC3-II/I (C), p62 (D), p-mTOR (normalized to total mTOR) (E) and total mTOR (F). Semi-quantitative analysis of CMA marker levels: LAMP2 (G) and GAPDH (H). Representative immunoblots of ALP markers in 12-month-old LRRK2-mutant mice (I). β-actin was used as housekeeping protein. Data are mean ± SEM of 8 mice per group and were analyzed using one-way ANOVA followed by the Bonferroni's test for multiple comparisons. *p<0.05, **p<0.01 different from WT mice.
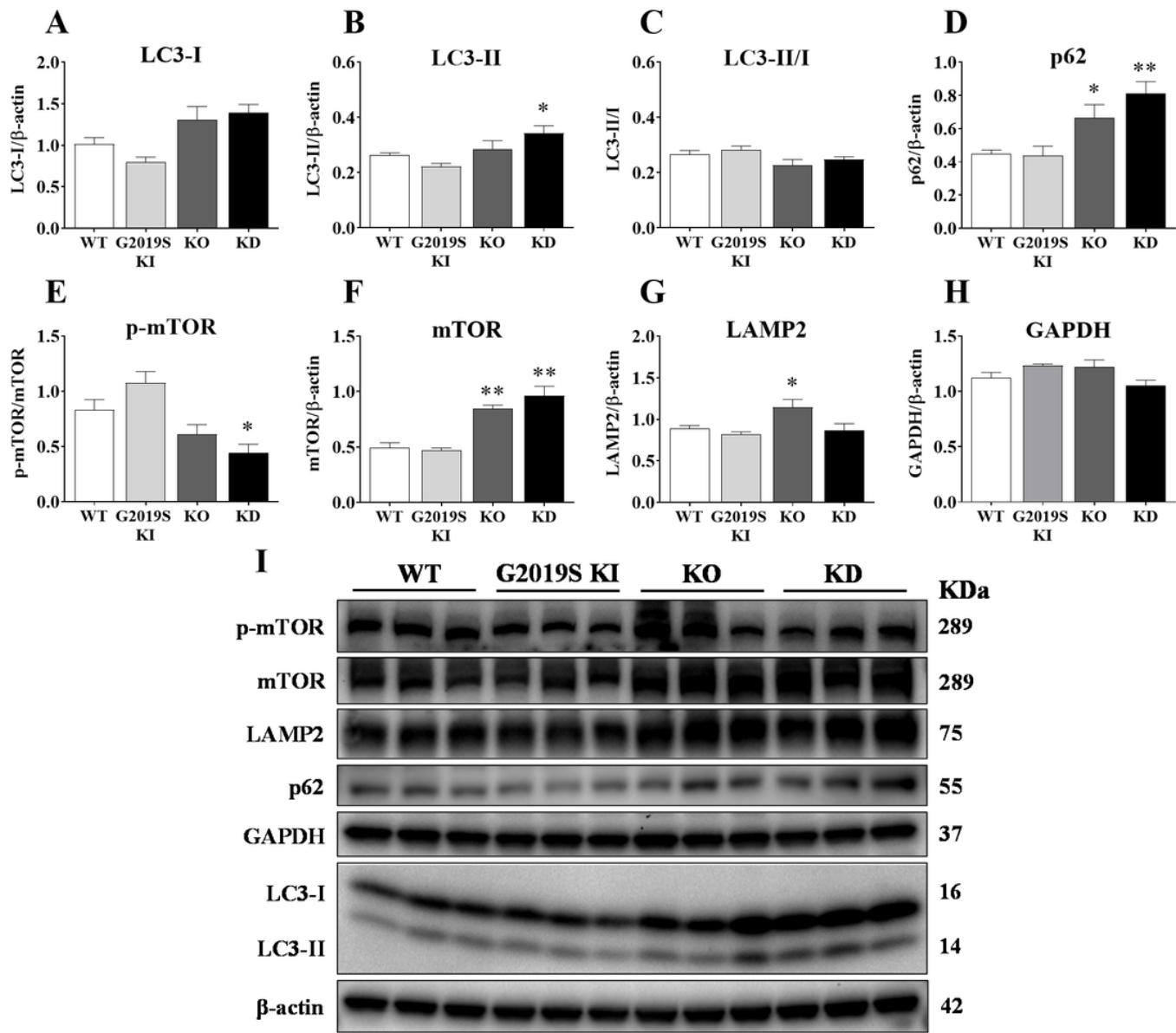
Figure 2

Immunoblot analysis of autophagy-lysosomal pathway (ALP) markers in 20-month-old LRRK2 mice. Striatum lysates from 20-month-old WT, G2019S KI, KO and KD mice. Semi-quantitative analysis of macroautophagy marker levels: LC3-I (A), LC3-II (B), LC3-II/I (C), p62 (D), p-mTOR normalized on total mTOR (E) and total mTOR (F). Semi-quantitative analysis of CMA marker levels: LAMP2 (G) and GAPDH (H). Representative immunoblots of ALP markers in 20-month-old LRRK2-mutant mice (I). β-actin was used as housekeeping protein. Data are mean ± SEM of 8 mice per group and were analyzed using one-way ANOVA followed by Bonferroni's test for multiple comparisons. *p<0.05; ** p<0.01 different from WT mice.
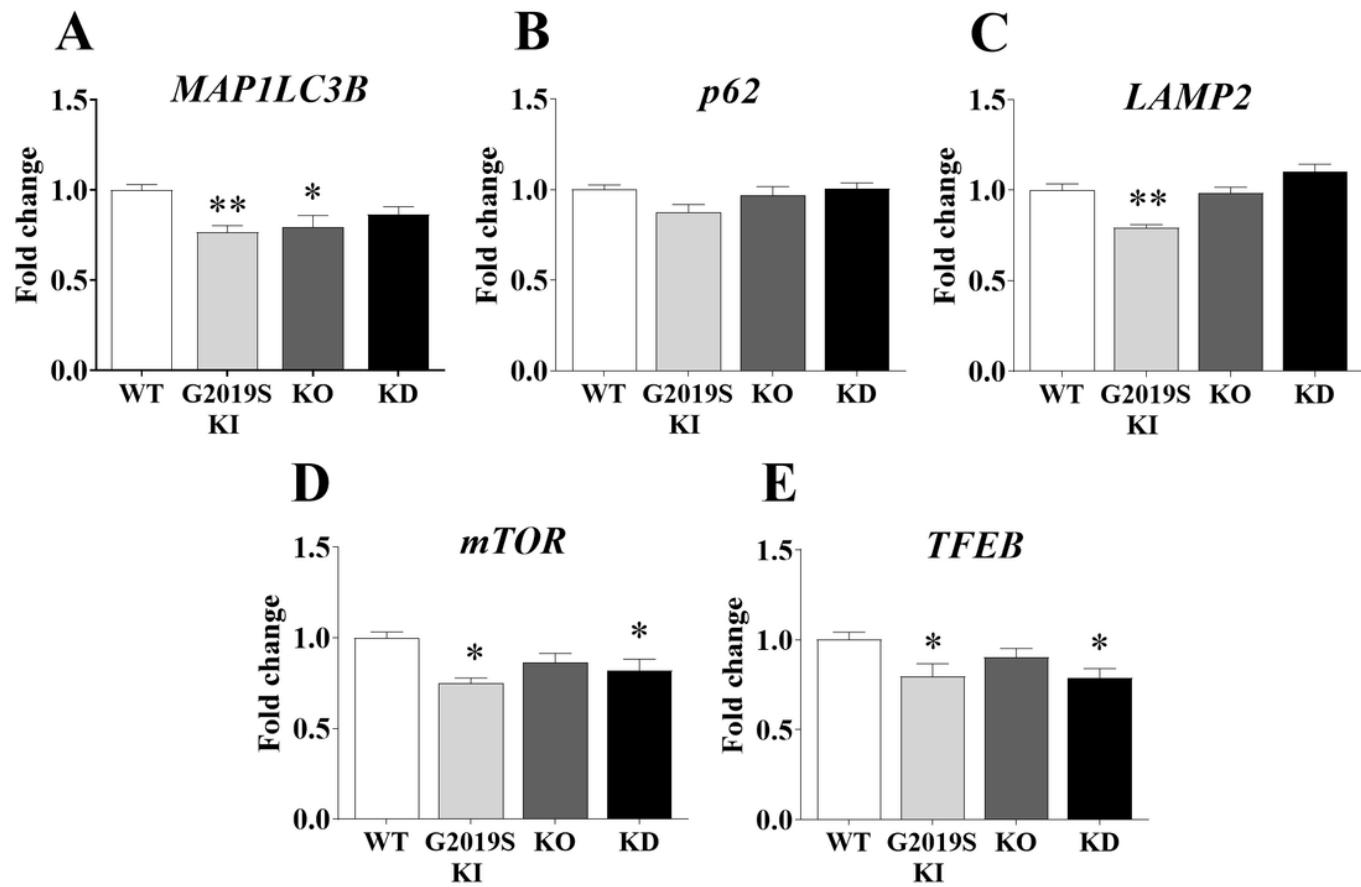
Figure 3

RT-qPCR analysis of autophagy-related gene expression in 12-month-old LRRRK2 mice. RNAs were isolated from striatal tissue of 12-month-old WT, G2019S KI, KO and KD mice. RT-qPCR analysis was performed to analyze the mRNA expression levels of MAP1LC3B (A), p62 (B), LAMP2 (C), mTOR (D), TFEB (E) among genotypes. ACT and HPRT were used as reference genes (Gong et al., 2016). Data are mean ±SEM of 8 mice per genotype. Statistical analysis was performed using one-way ANOVA followed by the Dunnett's test for multiple comparison. *p< 0.05, **p<0.01 different from WT mice.
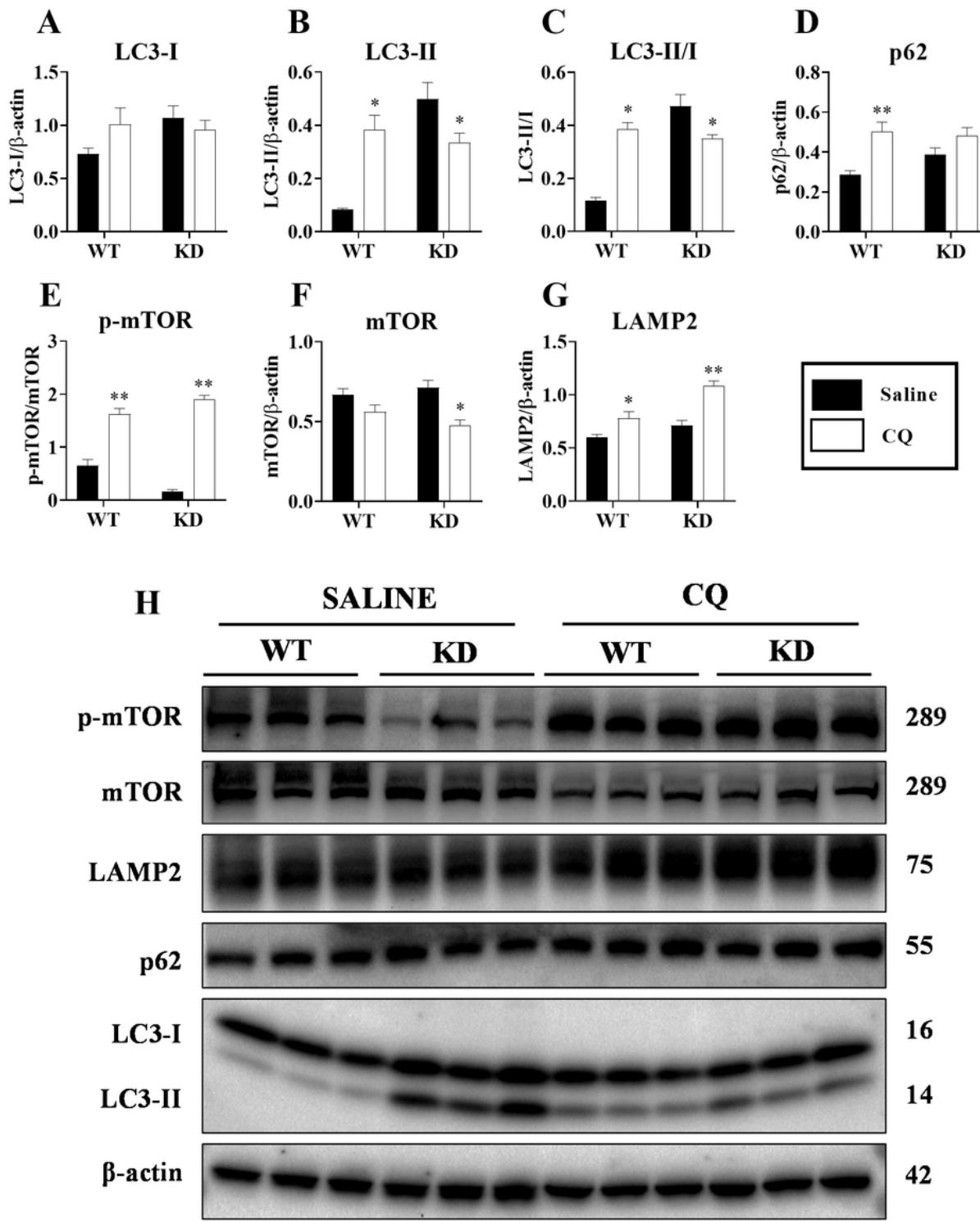
Figure 4

Autophagic flux assessment in 12-month-old WT and KD mice. Semi-quantitative analysis of macroautophagy marker levels: LC3-I (A), LC3-II (B), LC3-II/I (C), p62 (D), p-mTOR normalized on total mTOR (E) and total mTOR (F). Semi-quantitative analysis of CMA marker levels LAMP2 (G). Representative immunoblots of macroautophagy, mTOR activation and CMA markers (n=6) after CQ and saline administration (H). β-actin was used as housekeeping protein. Data are mean ± SEM. Statistical

analysis was performed using Student's t test, two-tailed for unpaired data. *p<0.05, **p<0.01 different from saline-treated mice.
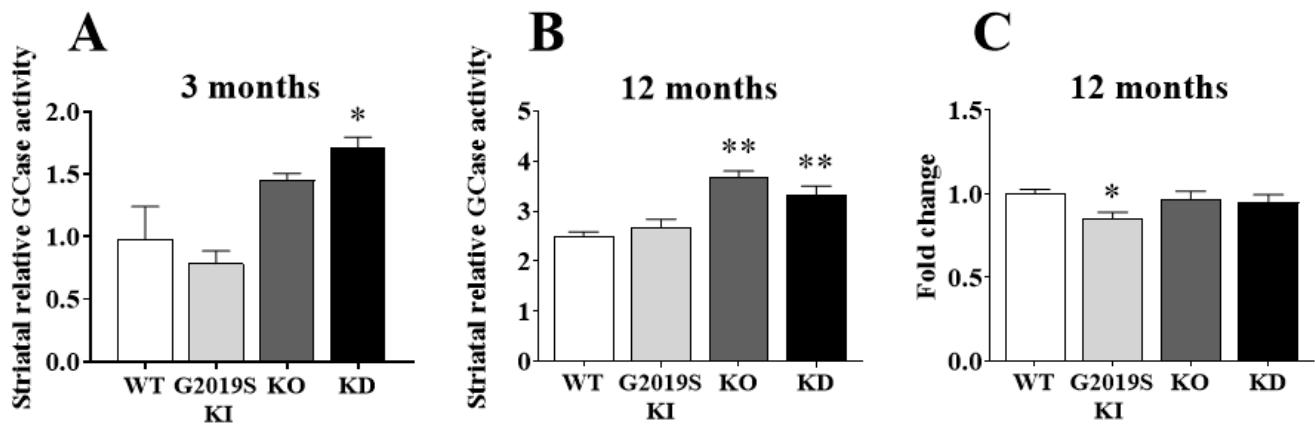

Figure 5

Relative striatal GCase activity in 3 and 12-month-old LRRK2 mice. Striatal tissue lysates isolated from 3-month-old (A) and 12-month-old (B) WT (n=6-8), G2019S KI (n=6-8), KO (n=6) and KD (n=6) mice were used to measure Relative GCase activity. Striatal GBA1 gene expression was assessed (n=8) at 12 months (C). ACT and HPRT were used as reference genes for RT-qPCR analysis. Data are mean ± SEM of n mice per group. For GCase activity assay, data were analyzed using one-way ANOVA followed by Bonferroni's test for multiple comparisons. *p<0.05, **p<0.01 different from WT mice. For RT-qPCR analysis, data were analyzed using one-way ANOVA followed by the Dunnett's test for multiple comparison. *p<0.05, **p<0.01 different from WT mice.
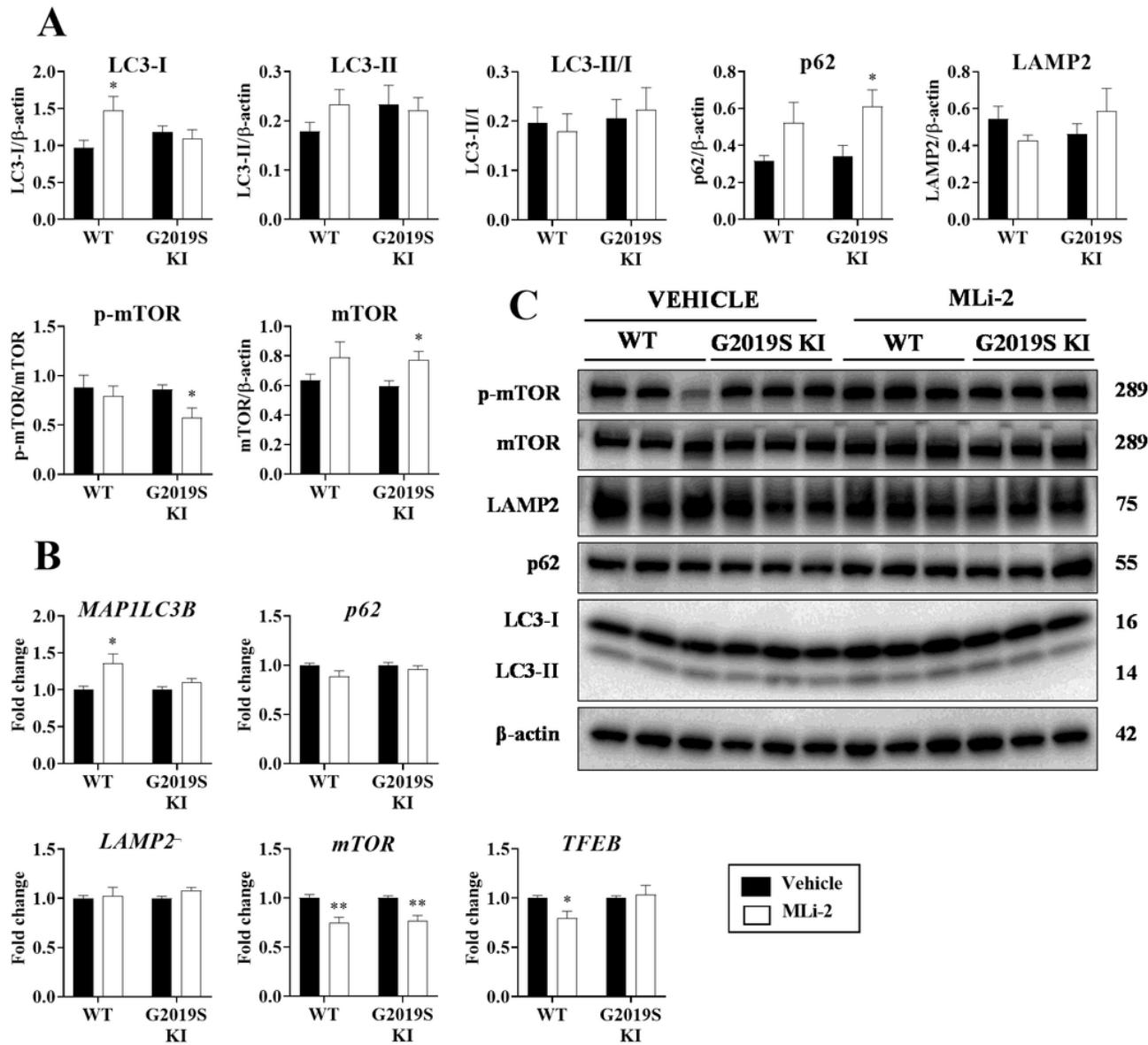
Figure 6

Sub-acute pharmacological inhibition of LRRK2 kinase activity in 12-month-old WT and G2019S KI mice. Mice were subacutely administered with the LRRK2 kinase inhibitor MLi-2 (5 mg/Kg i.p., once daily for 7 days) and sacrificed 4 hours after the last injection. A) Semi-quantitative analysis of macroautophagy markers (LC3-I, LC3-II, LC3-II/I ratio, p62, p-mTOR, mTOR) and CMA marker (LAMP2) levels, and representative immunoblots. B) RT-qPCR analysis of mRNA levels of MAP1LC3B, p62, LAMP2, mTOR and TFEB genes. β-actin was used as housekeeping protein and ACT and HPRT were used as reference genes. Data are mean ± SEM of 6 mice per group. Protein levels were analyzed using one-way ANOVA followed by the Bonferroni's test for multiple comparisons $*p < 0.05$, $**p < 0.01$ different from saline-treated mice. Transcript levels were analyzed using one-way ANOVA followed by the Dunnett's test for multiple comparison. $*p < 0.05$, $**p < 0.01$ different from saline-treated mice.
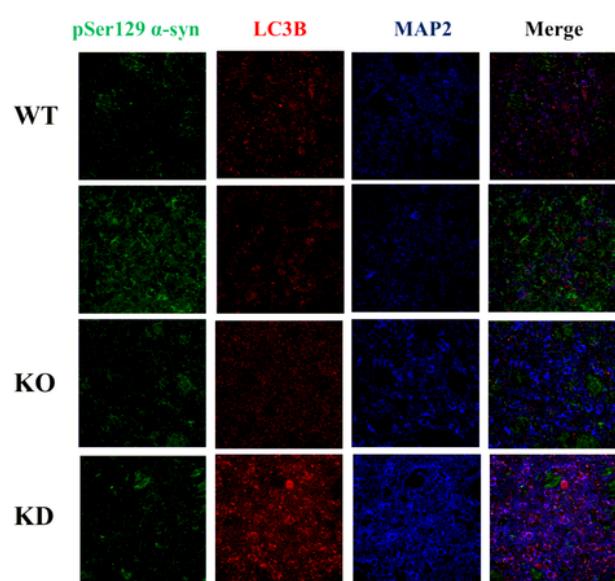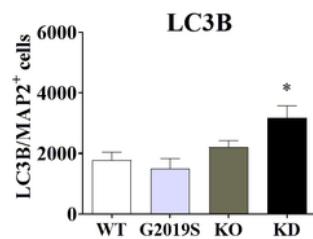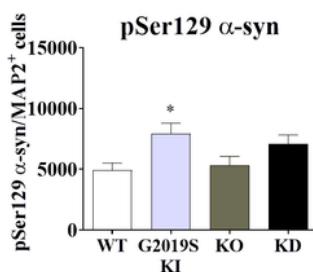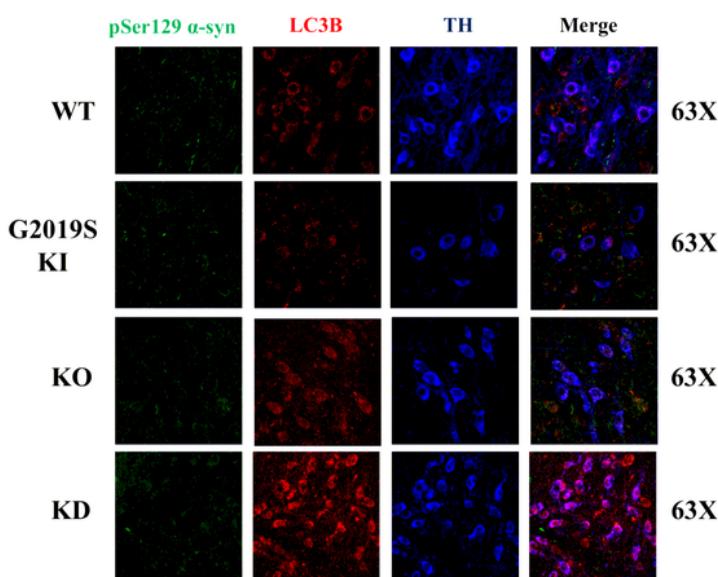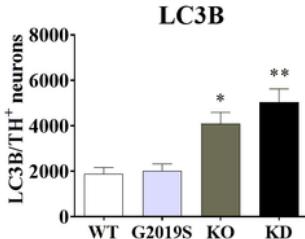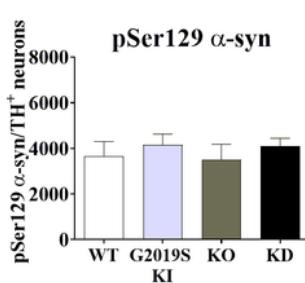
Figure 7

Immunofluorescence analysis of LC3B puncta and pSer129 α-syn inclusions in striatal MAP2+ and nigral TH+ neurons of 12-month-old LRRK2 mice. A) Representative immunofluorescence images and quantification of B) LC3B expression and C) pSer129 α-syn inclusions in striatal MAP+ cells. D) Representative immunofluorescence images and quantification of E) LC3B expression and F) pSer129 αsyn inclusions in nigral TH+ cells. The number of LC3B puncta was quantified within a mask image

made by the TH or MAP2 staining. Data are mean ± SEM of 6-8 mice per group and were analyzed using one-way ANOVA followed by the Bonferroni's test for multiple comparisons. *p<0.05, **p<0.01 different from WT mice.

Supplementary Files

This is a list of supplementary files associated with this preprint. Click to download.

- SupplfigAutophagy280521Final.docx